Supporting Information

Observation of molecular hydrogen produced from bridging hydroxyls on anatase TiO_2(101)

N. Aaron Deskins [b], Greg A. Kimmel [a] and Nikolay G. Petrik [a]

[a] Physical and Computational Sciences Directorate, Pacific Northwest National Laboratory, P.O. Box 999, Richland, Washington 99352, United States.

[b] Department of Chemical Engineering, Worcester Polytechnic Institute, 100 Institute Road, Worcester, MA, 01609, USA.

Additional Experimental Details

The anatase TiO_2 single crystal sample was mounted on a tantalum plate using high-temperature conducting cement (Aremco 865). Thin tantalum wires wrapped around the corners were used to restrain the sample in case the cement failed (see Figure S6a). The sample was annealed by resistively heating the base plate. The temperature was monitored by a K-type thermocouple spot-welded to the back of the base plate. Ramping the temperature at 2 K/s to obtain TPD spectra resulted in a significant thermal gradient between the base plate and the front surface of the 2 mm thick crystal, particularly at higher temperatures. We have performed a temperature calibration at various heating rates by analyzing zero-order TPD spectra of multilayer coverages of H_2O and CO_2 ices. For multilayers, the leading edges of the multilayer desorption features are independent of the ramp rate and can be compared with the standard vapor pressure data versus temperature.[1] These measurements were used to adjust the temperature reading made off the back of the base plate. The resulting uncertainty in the surface temperature at 200 K and 520 K is estimated to be ± 10 K and ± 35 K, respectively.

For electron irradiations, the electron beam was directed at 40° with respect to the sample normal. The incident energy of the electrons was 500 eV, and the instantaneous current densities were ~3.3×10^{15} $cm^{-2}s^{-1}$, as measured with a Faraday cup. The electron beam was smaller than the molecular beam spot size (~1.5 mm and 7.0 mm, respectively). To produce a

uniform electron fluence across the adsorbate films, the electron beam was rastered over an area slightly larger than the molecular beam spot, delivering 3.5 × 10^{13} cm^{-2} electrons per scan (at 0.4s/scan). The irradiation temperature was 100 K for all the results presented here.

For the IRAS experiments (see Figs. 2b and S2), p-polarized infrared (IR) light was incident on the TiO_2(101) single crystal at 20° relative to the $[10\bar{1}]$ azimuth (Figure S6b). The beam was incident at grazing incidence (~85° with respect to the surface normal, Fig. S6d) and detected in the specular direction. For p-polarized light, the electric field vector has components perpendicular and parallel to the surface. For the geometry used in current experiments, modes that are perpendicular to the surface show up as negative absorbance ("emission") peaks, while modes that are parallel to the surface show up as positive peaks.[2,3] Each individual IRAS experiment includes 6000 interferometer scans from the reference surface [i.e. clean anatase TiO_2(101)] and 6000 interferometer scans from the surface with the adsorbate layer. All the IRAS measurements were collected at ~ 30 K. The spectra presented are the average of 18 and 24 individual experiments for the annealed and irradiated surfaces, respectively. For s-polarized light, the electric field vector is parallel to surface and therefore, those spectra are sensitive to vibrations that have transition dipole moments parallel to the surface. For our system, the signal-to-noise ratio is worse for s-polarized light. Because of this and the expectation that the transition dipole moments for the surface hydroxyls are oriented primarily normal to the surface, s-polarized spectra were not investigated.

H_2 and H_2O desorption energies.

In order to determine H_2 and H_2O desorption energies at finite temperature from the DFT results we used an ab initio thermodynamics approach, which has been described previously.[4-7] In the case of a desorption process, the entropy of the gas phase species is much greater than the solid-state system. Thus, we can approximate the H_2 desorption free energy as follows:

$$\Delta G_{H2\text{-}desorption} \approx E_{surf} + G_{H2} - E_{surf+2HO}. \quad \text{(S1)}$$

All energies (E) are taken from DFT calculations. The free energy of H_2 is taken as

$$G_{H2} = E_{H2} + (PV)_{H2} - S_{H2}T. \quad \text{(S2)}$$

Again E_{H2} is taken from a DFT calculation. The PV and ST terms are taken from tabulated experimental data for H_2.[8,9] A similar expression can be used for H_2O desorption:

$$\Delta G_{H2O\text{-}desorption} \approx E_{surf+Vo} + G_{H2O} - E_{surf+2HO}. \quad \text{(S3)}$$

For the results shown in figure 4, the entropy and pressure contributions in Equation S2 are referenced to a pressure of 1 bar. At the low pressures relevant for the UHV experiments, the entropic contributions make the gas phase species even more favorable. However, this does not change the conclusion that H_2 production is favored at high temperatures.

Table S1. Comparison of various DFT calculations for surface H diffusion. The reaction energies and activation energies are shown for each step.

Process	**ΔE (eV)**	**E_{act} (eV)**	**Source**
$HO_b \rightarrow HO_{3c\text{-}1}$	0.98	-	Islam et al.[10]
$HO_b \rightarrow HO_{3c\text{-}1}$	0.50	0.96	Aschauer et al.[4]
$HO_b \rightarrow HO_{3c\text{-}1}$	1.05	1.40	Current Work
$2\ HO_b \rightarrow H_2 + 2\ O_b$	0.79	2.87	Raghunath et al.[11]
$2\ HO_b \rightarrow H_2 + 2\ O_b$	-0.26	2.01	Aschauer et al. [4]
$2\ HO_b \rightarrow H_2 + 2\ O_b$	0.30	--	Current Work
$HO_b + HO_{3c\text{-}1} \rightarrow H_2 + O_b + O_{3c\text{-}1}$	-0.32	1.48	Aschauer et al. [4]
$HO_b + HO_{3c\text{-}1} \rightarrow H_2 + O_b + O_{3c\text{-}1}$	-0.98	1.22	Current Work

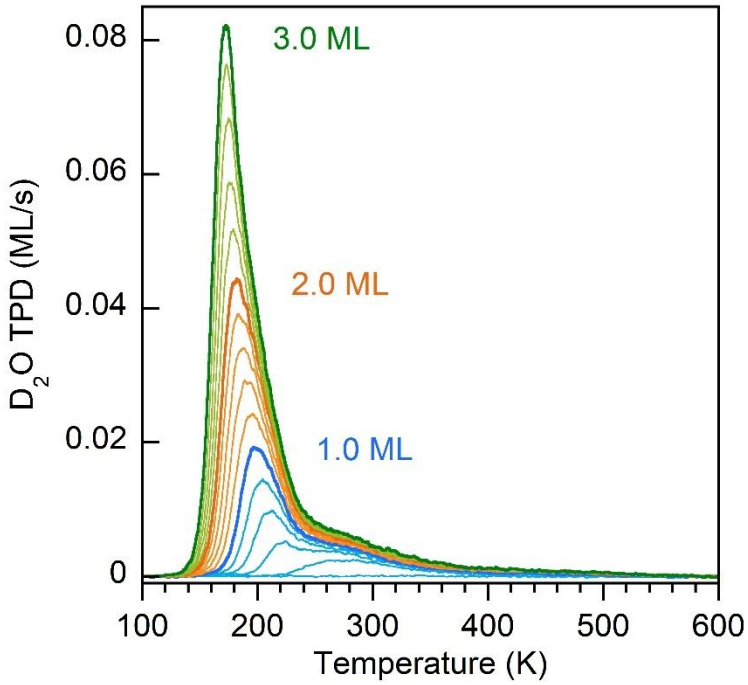

Figure S1. TPD spectra D_2O (20 amu) adsorbed on TiO_2(101). Spectra are shown for coverages from 0.0 to 3.0 ML in 0.2 ML increments The ramp rate was 2K/s.

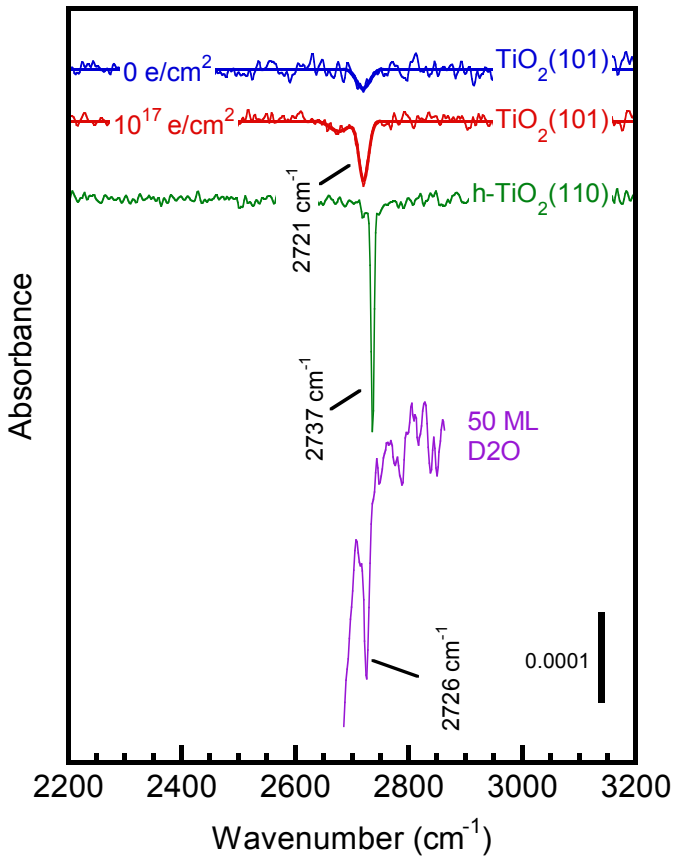

Figure S2. Comparison of p-polarized IRAS spectra of non-hydrogen bonded OD groups on anatase TiO_2(101), rutile TiO_2(110) and amorphous solid D_2O. The blue (red) line shows the spectrum for sputtered and annealed (electron-irradiated) TiO_2(101) after dosing 1 ML D_2O at 100 K and briefly annealing to 410 K. (These are the same spectra shown in Fig. 2b.) The spectra of bridging hydroxyls, DO_b, on rutile TiO_2(110)[12] (green line) and the non-hydrogen bonded OD's on the surface of a 100 ML amorphous solid D_2O film (purple line) are shown for comparison. For DO_b on rutile TiO_2(110), the resolution was 1 cm^{-1}, while the other spectra were obtained with 4 cm^{-1} resolution. The amorphous solid D_2O film was deposited at 50 K.

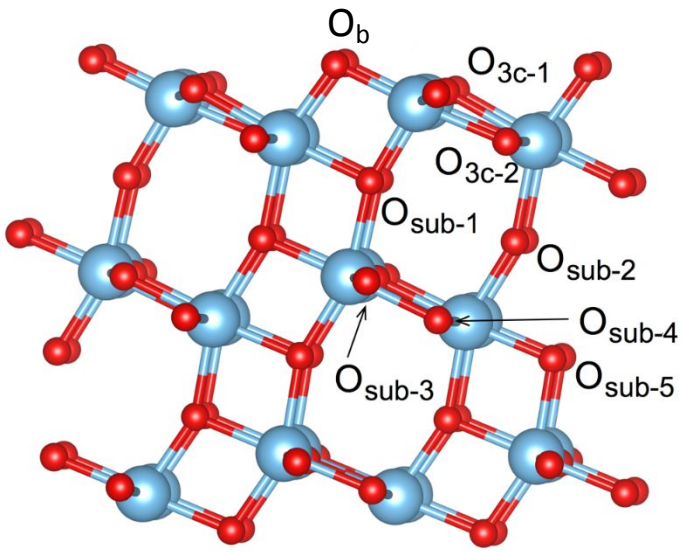

Figure S3. The (101) anatase slab used in this work. Surface two-coordinated (O_b) and three-coordinated (O_{3c-1}, $O3_{c-2}$) O atoms are indicated. Sub-surface atoms are also indicated.

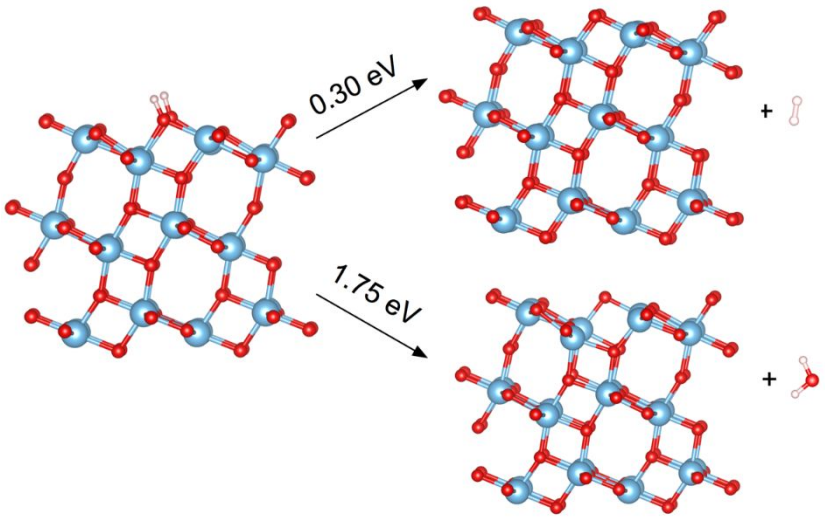

Figure S4. Geometries and desorption energies for H_2 and H_2O desorption from the (101) surface.

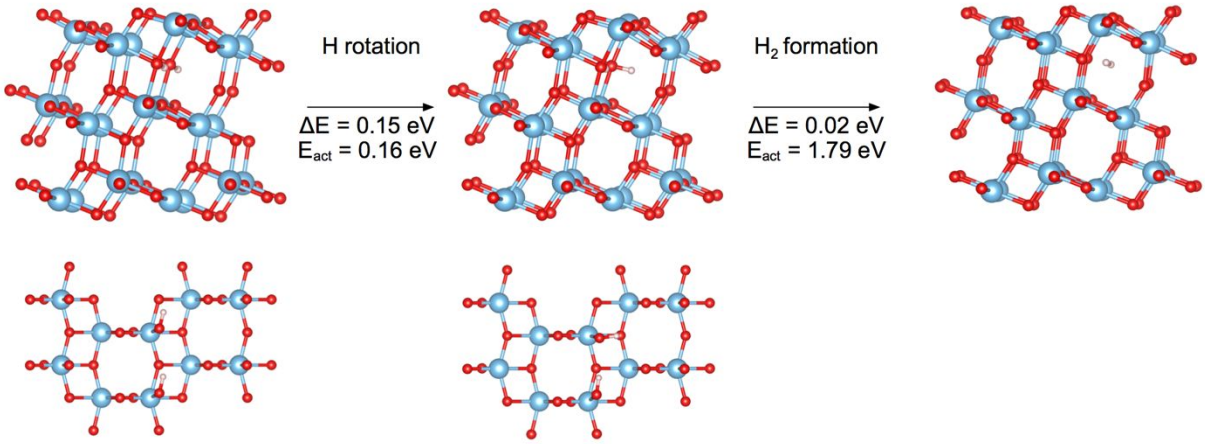

Figure S5. Calculated pathways for sub-surface formation of H_2. The first step involves the rotation of one of the H atoms to bring it closer to the other H atom. The second step involves O-H bond breaking and H-H bond formation.

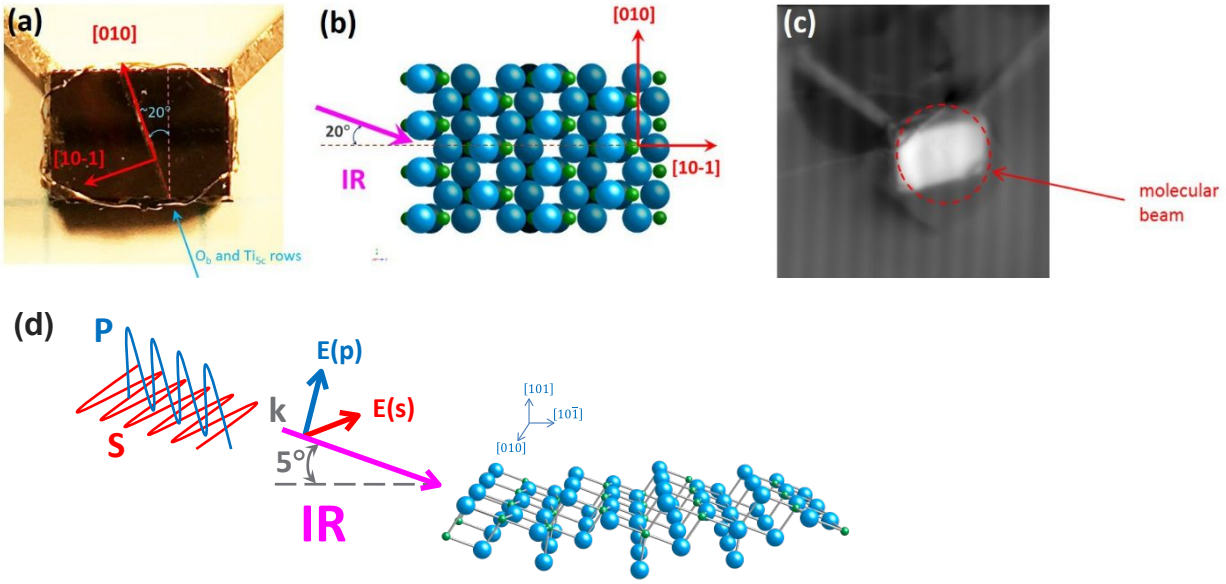

Figure S6. (a) Picture of the anatase TiO_2(101) sample (7×5 ×2 mm^3) mounted on a tantalum plate holder. Thin tantalum wires are visible at the corners. Note that the [010] and $[10\bar{1}]$ directions are rotated 20° relative to the sides of the crystal. (b) The IR beam was incident along an azimuth rotated 20° to the $[10\bar{1}]$ direction (i.e. the projection of the IR beam's **k** vector in the plane of the surface was parallel to the longer (7 mm) side of the crystal). The IR beam was incident at glancing angle to the (101) surface (5°). (c) Image of the sample with a dosed H_2O film (white spot). The image was made by rastering the electron beam over a wide area and measuring the scattered electrons reaching an electrode in vacuum chamber. Changes in the electron scattering off various surfaces, including the water film, produce the contrast for the image. The molecular beam ∅ 7.3 mm (umbra), centered on the sample and larger than the sample. d) Schematic for IRAS geometry on TiO_2(101). For s-polarized light, the electric field, E(s), is parallel to the (101) surface and perpendicular to the IR beam direction shown in (b). For the geometry shown, s-polarized spectra are sensitive to vibrations with a transition dipole moment that has a component parallel to surface and perpendicular to the direction of the IR beam. For p-polarized light, the electric field, E(p), has components both normal and parallel to the surface. Thus p-polarized spectra are sensitive to transition dipole moments perpendicular to the (101) surface and parallel to the surface in the direction of the IR beam.

Supplemental References.

(1) Schlichting, H.; Menzel, D. Techniques for attainment, control, and calibration of cryogenic temperatures at small single-crystal samples under ultrahigh vacuum. *Rev. Sci. Instrum.* **1993**, *64*, 2013-2022.

(2) Chabal, Y. J. SURFACE INFRARED-SPECTROSCOPY. *Surf. Sci. Rep.* **1988**, *8*, 211-357.

(3) Kimmel, G. A.; Baer, M.; Petrik, N. G.; VandeVondele, J.; Rousseau, R.; Mundy, C. J. Polarization- and Azimuth-Resolved Infrared Spectroscopy of Water on TiO_2(110): Anisotropy and the Hydrogen-Bonding Network. *J. Phys. Chem. Lett.* **2012**, *3*, 778-784.

(4) Aschauer, U.; Selloni, A. Hydrogen interaction with the anatase TiO2(101) surface. *Physical Chemistry Chemical Physics* **2012**, *14*, 16595-16602.

(5) Deskins, N. A.; Lauterbach, J.; Thomson, K. T. Lifting the Pt[100] surface reconstruction through oxygen adsorption: a density functional theory analysis. *The Journal of chemical physics* **2005**, *122*, 184709-184709.

(6) Iyemperumal, S. K.; Fenton, T. G.; Gillingham, S. L.; Carl, A. D.; Grimm, R. L.; Li, G.; Deskins, N. A. The stability and oxidation of supported atomic-size Cu catalysts in reactive environments. *The Journal of Chemical Physics* **2019**, *151*, 054702.

(7) Reuter, K.; Scheffler, M. Composition and structure of the RuO2(110) surface in an O-2 and CO environment: Implications for the catalytic formation of CO2. *Physical Review B* **2003**, *68*, 045407.

(8) Cengel, Y. A.; Boles, M. A.; New York: McGraw-Hill Education: 1997.

(9) Chase, M. W. *NIST-JANAF thermochemical tables*; Fourth ed.; American Chemical Society: Washington, D.C., 1998.

(10) Islam, M. M.; Calatayud, M.; Pacchioni, G. Hydrogen Adsorption and Diffusion on the Anatase TiO2(101) Surface: A First-Principles Investigation. *The Journal of Physical Chemistry C* **2011**, *115*, 6809-6814.

(11) Raghunath, P.; Huang, W. F.; Lin, M. C. Quantum chemical elucidation of the mechanism for hydrogenation of TiO2 anatase crystals. *The Journal of Chemical Physics* **2013**, *138*, 154705.

(12) Petrik, N. G.; Kimmel, G. A. Reaction Kinetics of Water Molecules with Oxygen Vacancies on Rutile TiO_2(110). *J. Phys. Chem. C* **2015**, *119*, 23059-23067.